Pizzagalli and David *Materials Theory* (2021) 5:5
https://doi.org/10.1186/s41313-021-00028-2

Materials Theory

ORIGINAL ARTICLE Open Access

Surface stress calculations for nanoparticles and cavities in aluminum, silicon, and iron: influence of pressure and validity of the Young-Laplace equation

Laurent Pizzagalli* and Marie-Laure David

*Correspondence:
laurent.pizzagalli@univ-poitiers.fr
Departement of Physics and Mechanics of Materials, Institut P', CNRS UPR 3346, Université de Poitiers, SP2MI, Boulevard Marie et Pierre Curie, TSA 41123, 86073 Poitiers Cedex 9, France

Abstract

This study is dedicated to the determination of the surface energy and stress of nanoparticles and cavities in presence of pressure, and to the evaluation of the accuracy of the Young-Laplace equation for these systems. Procedures are proposed to extract those quantities from classical interatomic potentials calculations, carried out for three distinct materials: aluminum, silicon, and iron. Our investigations first reveal the increase of surface energy and stress of nanoparticles as a function of pressure. On the contrary we find a significant decrease for cavities, which can be correlated to the initiation of plastic deformation at high pressure. We show that the Young-Laplace equation should not be used for quantitative predictions when the Laplace pressure is computed with a constant surface energy value, as usually done in the literature. Instead, a significant improvement is obtained by using the diameter and pressure-dependent surface stress. In that case, the Young-Laplace equation can be used with a reasonable accuracy at low pressures for nanoparticles with diameters as low as 4 nm, and 2 nm for cavities. At lower sizes, or high pressures, a severely limiting factor is the challenge of extracting meaningful surface stress values.

Keywords: Theory, Young-Laplace equation, Surface stress, Nanoparticles, Cavities

Introduction

Many physical laws have been discovered following the observation of phenomena occurring at macroscale, where the matter is conveniently described as a continuum. The question of their validity arises when one or several dimensions of materials are decreased down to the nanoscale, i.e., when the discrete character of matter cannot be neglected. As it stands, it is likely that the answer critically depends on which physical law is used. Considering for instance mechanical contacts, it is now well established that using continuum models at the nanoscale could lead to significant errors compared to a more realistic atomistic description (Vergeles et al. 1997; Tanguy et al. 2004; Luan and Robbins 2005; Armstrong and Peukert 2012; Bel Haj Salah et al. 2017; Yang et al. 2017). Conversely,

it has recently been shown that the acoustic vibrations of nanoparticles could be reliably predicted from continuum laws even for sub-nanometric dimensions (Maioli et al. 2018). These contradictory observations then emphasize the need for investigations on a case-by-case basis.

A famous continuum law is the Young-Laplace equation (YLE), which describes the pressure difference ΔP due to capillary forces between two phases separated by a curved interface by:

$$\Delta P = \frac{2\Gamma}{R} \tag{1}$$

where Γ is the surface tension (or surface stress) and R is the curvature radius. The right term will be called Laplace pressure in the remaining of this paper. Although the YLE was originally derived for an interface between fluids, using this equation for solid/fluid interface is relatively common in the scientific literature. For instance, the lattice parameter shrinking in nanoparticles of decreasing diameters is successfully explained on the basis of an increasing Laplace internal pressure (Medasani et al. 2007; Wolfer 2011). Nonetheless the validity range of the YLE remains an open question. Lower size thresholds of 2 nm and 4.8 nm for nanoparticles were reported in the literature (Hawa and Zachariah 2004; Cui et al. 2015)

In a nuclear material context, the YLE is often used to estimate the internal pressure of noble gas bubbles embedded in various materials (Jäger et al. 1982; Fréchard et al. 2009; Stoller and Osetsky 2014; Cui et al. 2015). In conditions of mechanical equilibrium, this pressure is predicted to increase for decreasing bubble size. Measurements of the pressure inside single nanometric bubbles have been performed (Taverna et al. 2008; David et al. 2014; Alix et al. 2015; Schierholz et al. 2015), which could allow for assessing the validity of the YLE in this specific context. Hence, an inverse linear relation has been determined for He bubbles in steel (Fréchard et al. 2009). However, studies of He bubbles in silicon point to an absence of relation between size and pressure (Dérès et al. 2017; Alix et al. 2018; Ono et al. 2019). It is not clear whether the cause of the discrepancy are the experimental conditions or the YLE being not valid at this scale.

It is also noteworthy that Γ in the YLE is very often assumed to be equal to the surface energy by default, since available information on surface stress values is scarce. For a solid, the surface stress is a two-dimensional second rank tensor, and it is related to the scalar surface energy through the so-called Shuttleworth equation (Shuttleworth 1950; Müller and Saùl 2004; Makkonen 2012; Müller et al. 2014):

$$\Gamma_{ij} = \gamma\delta_{ij} + \frac{\partial\gamma}{\partial\varepsilon_{ij}} \tag{2}$$

where δ_{ij} is the Kronecker symbol and ε is the surface strain tensor. Γ becomes a scalar equal to the surface energy γ only for a fluid/fluid interface, which is obviously not the case for nanoparticles or bubbles embedded in a solid matrix. This is another potential source of errors that should be evaluated.

At last, the influence of pressure on surface stress and on the validity of the YLE remains to be elucidated. Recently, Jelea showed that the surface stress is in fact not constant for the helium/steel interface, with a non-linear strain dependence (Jelea 2018). Large pres-

sures greater than 10 GPa have been reported in helium filled nanometric bubbles formed by implantation (Dérès et al. 2017; Alix et al. 2018). Nanoparticles also can be subjected to similar or even higher pressures in dedicated experiments (Bai et al. 2019).

In this work, we first aim at determining the surface stresses for nanoparticles and embedded cavities as a function of size and applied pressure, by performing interatomic potential calculations. We use cavities with an applied internal pressure to model pressurized bubbles. To reach comprehensive conclusions, three different materials, aluminum, iron, and silicon, are considered in this work. These results are next used to assess the validity of the YLE as a function of system size and applied pressure. The paper is organized according to the following structure. The models and the details of the numerical simulations are first described in the "Simulations" section. The methods used to compute the surface stress from these simulations and the results are described in the "Surface energy and stress" section. In the "Validity of the Young-Laplace equation" section, the validity of the YLE as a function of nanoparticle/cavity size and applied pressure for the different materials is assessed. Finally, we conclude in the last section.

Simulations

The two models used in the numerical simulations are depicted in Fig. 1. The spherical nanoparticles and cavities are generated by carving bulk materials with FCC (Al), BCC (Fe), or cubic diamond (Si) crystalline structures. Diameters for both models range from 2 nm to 20 nm. The dimension of the cubic crystal encompassing the cavity is chosen so as to get at least 10 nm between the cavity surface and the crystal edges. It then ensures that there are at least 20 nm betwen the cavity and its replicas when periodic boundary conditions are applied.

All our calculations were performed using the LAMMPS package (Plimpton 1995). Al and Fe interactions are modeled with embedded atom model potentials (Aslanides and Pontikis 1998; Proville et al. 2012), whereas a Stillinger-Weber potential is used for silicon (Pizzagalli et al. 2013). Table 1 lists various properties computed with these potentials for the three materials.

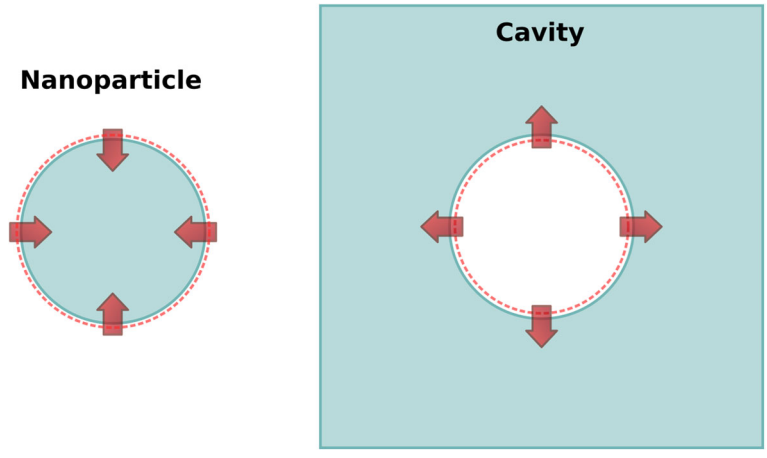

Fig. 1 Models used in simulations. The dashed red line represents the repulsive spherical force field which mimics the effect of an isotropic compression on a nanoparticle (left), and of a pressurized bubble on its surrounding medium (right)

Table 1 Bulk atomic volume v_b and cohesive energy ε_b, elastic constants and shear modulus $G = (C_{11} - C_{12} + 3C_{44})/5$ for the three materials/potentials used in the study

	v_b (Å^3)	ε_b (eV)	C_{11} (GPa)	C_{12} (GPa)	C_{44} (GPa)	G (GPa)
Al	16.243	-3.336	116	61	30	29
Fe	11.151	-4.122	243	145	116	89
Si	20.023	-4.630	156	80	58	50

The compression of a nanoparticle is obtained by adding a spherical repulsive force field centered on the nanoparticle, with a magnitude given by:

$$F_i(r_i) = -K(r_i - R)^2 \tag{3}$$

with r_i the distance between the atom i and the center. The force on atom i is applied only if $r_i > R$, thus allowing for compression by decreasing R. The parameter K is equal to 10^3 eV Å^{-3}. A similar approach is employed to obtain a pressure on the cavity surface. In that case, the force on atom i is applied only if $r_i < R$. Increasing R thus allows for an growing pressure on the cavity surface. Using such a force field leads to well controlled static simulations, with normal forces applied on all matrix or nanoparticle surface atoms.

The compression is performed at 0 K according to the following procedure for each run: an initial force relaxation of the nanoparticle/cavity is performed. Next, the repulsive force field is activated, with an initial R value slightly larger (lower) than the nanoparticle (cavity) radius. R is successively decreased for the nanoparticle, or increased for the cavity, with a complete force relaxation between each increment. For each converged state the repulsive force field is temporarily deactivated and the now non-zero atomic forces are recorded, for reasons that will become apparent later in the paper. Note that for each R value, the nanoparticle (cavity) is first contracted (expanded) by a radial translation of each atom with a magnitude depending on its distance to the surface and the R increment. This allows for preventing large spurious displacements at the surface when the relaxation starts. In all runs, forces relaxation is achieved by using the FIRE algorithm (Bitzek et al. 2006) with a timestep of 10 fs, and a force threshold of 10^{-4} eV Å $^{-1}$. The same procedure is used for all three materials. However, for silicon, extra steps are made to ensure an initial physically realistic surface. Before compression, surface atoms with a coordination equal to 1 are first removed. Thereafter, a molecular dynamics simulation at 600 K and with a time step of 1 fs is carried out during 10 ps to foster reconstruction. The temperature is next lowered from 600 K to 0 K during 1ps, before starting the compression.

At each R increment, the position, energy, force, Voronoi volume and stress tensor of all atoms of the relaxed system are recorded. In LAMMPS, the formalism allowing for computing the atomic stress tensor is detailed in Ref. Thompson et al. (2009). At 0 K, one first computes the following quantity for a given atom:

$$\mathbf{s} = -\Sigma \mathbf{r} \otimes \mathbf{F} \tag{4}$$

the summation being over atoms interacting with this specific atom. $\mathbf{s}$ is a per-atom tensor, whose components are expressed in energy unit. The sum of $\mathbf{s}$ over all atoms in the system, divided by the total volume, yields the stress tensor of the system $\boldsymbol{\sigma} = \Sigma \boldsymbol{s}/V$ in pressure unit. It is also possible to calculate an atomic stress tensor in pressure unit by dividing $\mathbf{s}$ by the atomic volume, which is not a clearly defined quantity. In the literature it is usually estimated from a Voronoi spatial decomposition, an efficient and rigorous approach except for surface atoms.

Surface energy and stress: methods

Surface energy and stress are by definition the excess quantities of bulk energy and stress due to the presence of a surface (Cammarata 1994). The surface energy γ is usually computed using a slab model and the formula

$$\gamma = \frac{1}{2S}(E - N\varepsilon_0) \tag{5}$$

where S is the slab surface, E the slab energy, N the number of atoms in the slab and ε_0 the reference (bulk) energy of a single atom. The Eq. (5) requires atomic energies to be defined (for an approach using only total energies, see Ref. Needs (1987) for instance).

By the same logic, the surface stress Γ can be computed for a slab according to

$$\Gamma = \frac{V}{2S}(\boldsymbol{\sigma} - \boldsymbol{\sigma}_0) \tag{6}$$

with V the volume of the slab, $\boldsymbol{\sigma}$ the slab stress tensor and $\boldsymbol{\sigma}_0$ the reference bulk stress tensor. Data for various metals and silicon are reported (Jiang et al. 2001; Medasani et al. 2007; Wolfer 2011; Needs 1987; Payne et al. 1989; Swaminarayan et al. 1994; Hecquet 2013). If atomic stress tensor and volume can be defined, as it is the case in the present work, the previous equation can be written as

$$\mathbf{\Gamma} = \frac{1}{2S}(\Sigma \boldsymbol{s} - V\boldsymbol{\sigma}_0) = \frac{1}{2S}\left(\Sigma \boldsymbol{s} - V\frac{\boldsymbol{s}_0}{\nu_0}\right) \tag{7}$$

the summations being over all atoms, and ν is the atomic volume.

Nanoparticle

We now focus on the general problem of the calculation of surface energy and stress for nanoparticles. For surface stress, published methods rely on the use of thermodynamics, elasticity theory, or the YLE (Jiang et al. 2001; Luo and Hu 2013; Wolfer 2011; Medasani et al. 2007; Lazzari et al. 2016). Hereinafter we propose an approach allowing for the computation of Γ directly from atomistic calculations. The general Eqs. (5)-(7) can be used as long as atomic quantities (energies, stresses, volume) are defined, and taking into account the presence of a unique surface:

$$\gamma = \frac{1}{S}(E - N\varepsilon_0) \tag{8}$$

$$\mathbf{\Gamma} = \frac{1}{S}\left(\Sigma \boldsymbol{s} - V\frac{\boldsymbol{s}_0}{\nu_0}\right) \tag{9}$$

The volume V and surface S of the nanoparticle are required in Eqs. (8)-(9). These quantities can not be unambiguously defined at the atomic level. A usual remedy to this issue is to assume that surface atoms occupy the same volume than in the bulk (i.e., $\nu_0 = \nu_b$, Table 1), whereas Voronoi volumes are used for other atoms. V is then easily obtained as $\Sigma\nu$. Assuming that the nanoparticle is perfectly spherical, the diameter $D = (6V/\pi)^{\frac{1}{3}}$ and the surface $S = \pi D^2$ can be easily computed. Note that we also tested another approach to determine V, where we assumed that the volume of surface atoms was equal to the volume of atoms in the center of the nanoparticle, but the differences in results were negligible.

The calculation of the surface energy with Eq. (8) is now straightforward. For surface stress, we first focus on the atomic stress tensor which is output in (x, y, z) cartesian coordinates by LAMMPS. For a spherical nanoparticle, spherical coordinates (r, θ, ϕ) are obviously more convenient. Assuming perfect isotropy, the two-dimensional tensor $\mathbf{\Gamma}$ in spherical coordinates is fully characterized by a single value since θ and ϕ components

are equal. To obtain $\boldsymbol{s}$ in spherical coordinates for a given atom, we first determine the vector connecting this atom and the nanoparticle center. We compute the rotation matrix orienting this vector to the cartesion $\hat{z}$ axis, using the Rodrigues formula (The rotation angle is obtained from the scalar product of the vector defining the atom position and the ẑ axis. The cross product of these two vectors define the rotation axis). This matrix is next used to transform the atomic stress tensor in spherical coordinates for this specific atom. This operation is performed for all atoms in the nanoparticle, allowing for computing $\Sigma\boldsymbol{s}$. Note that the resulting tangential axis are different from one atom to another, and the summation over all atoms leads to $\Sigma\boldsymbol{s}_\theta \simeq \Sigma\boldsymbol{s}_\phi$, i.e., similar tangential components. The largest differences occurred for silicon, with a relative difference of at most 6%. For aluminum, values are always numerically equal. In all cases, the final value is taken to be the average of the two tangential components.

The second quantity to estimate is $\boldsymbol{\sigma}_0 = \boldsymbol{s}_0/\nu_0$ in Eq. (9). According to elasticity theory, the stress tensor is constant in an homogeneous sphere and an isotropic strain (Timoshenko and Goodier 1951). This property is verified for a nanoparticle except in the vicinity of its surface. Figure 2 shows the radial variation of $\boldsymbol{\sigma}$ and of the atomic energy. Stress diagonal components become constant about 10 Å (about 6 Å for the energy) from the surface (values of off-diagonal stress components, not shown, are zero as expected). The reference values $\boldsymbol{\sigma}_0$ and ε_0 are then chosen from the center of the nanoparticle. All quantities in Eq. (9) being determined, it is possible to compute the scalar surface stress as $\Gamma = (\Gamma_{\theta\theta} + \Gamma_{\phi\phi})/2$.

Cavity

We showed for the nanoparticle that it is possible to compute the surface energy and stress directly from the calculations. The task is slightly more complicated for the cavity since the applied load produces an inhomogeneous strain field, decreasing from the cavity surface with an inverse cubic radial dependence (Mura 1987; Jelea 2018) (Fig. 2). The

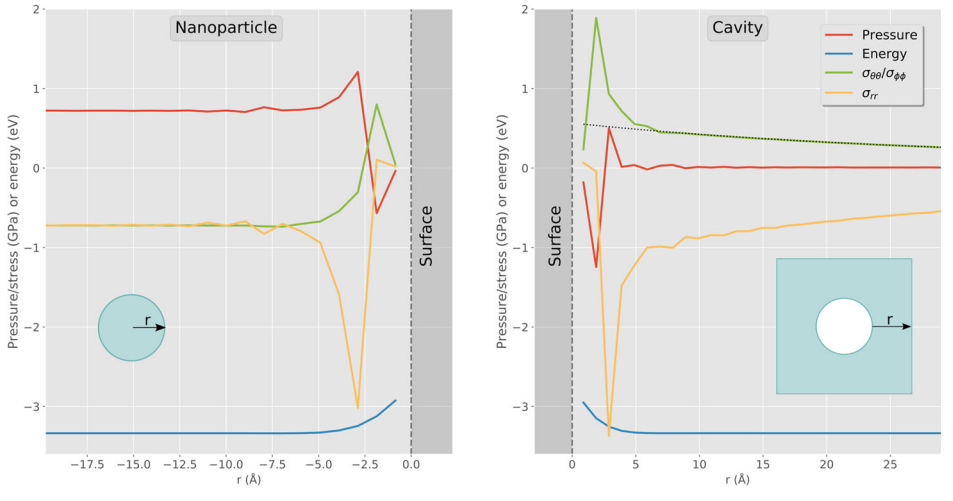

Fig. 2 Example of atomic energy, pressure, and diagonal stress tensor components variations in a 20 nm diameter aluminum nanoparticle (left) and cavity (right) as a function of the radial distance from the center, for two arbitrary applied pressures. All quantities are radial averages made in 1 Å thick shells. The vertical dashed lines indicate the position of the surface assuming perfectly spherical systems and a surface atom volume equal to the bulk atomic volume. The dotted line is a fit made with the expression α/r^3 and excluding data close to the surface

surface energy of the cavity can still be determined by subtracting the elastic energy due to compression. In principle, it is possible to numerically compute this energy using stress and strain fields (Hirth and Lothe 1982). However as a first step, it is more convenient to use the analytical expression provided by isotropic elasticity theory (Mura 1987; Pizzagalli et al. 2014). Eq. (5) then becomes

$$\gamma = \frac{1}{S}\left(E - N\varepsilon_0 - 8\pi G(R - R_0)^2 R_0\right) \tag{10}$$

R is the radius of the cavity with the applied load, which is determined using the same approximation for surface atoms than in the previous section. R_0 is the cavity radius before the load is applied. An open question, especially for the smallest cavities, is whether one should determine R_0 before or after force relaxation (and cavity expansion/contraction due to Laplace forces). In the present work, R_0 is computed after force relaxation. G is the shear modulus and ε_0 is equal to ε_b, using values reported in Table 1.

To determine the surface stress, we rewrite Eq. (7) as

$$\mathbf{\Gamma} = \frac{1}{S}\Sigma\left(\boldsymbol{s} - \nu\boldsymbol{\sigma}^{el}\right) \tag{11}$$

the summation being as usual over all atoms. The cavity surface S can be determined from the cavity volume V by assuming a spherical shape. To obtain V, the sum of atomic volumes for all atoms, assuming that surface atoms have the same volume than bulk atoms, is subtracted from the supercell volume. $\boldsymbol{\sigma}^{el}$ is the elastic atomic stress tensor associated with the cavity under load. This elastic contribution to the full stress tensor is subtracted from the atomistic calculations in Eq. (11). In spherical coordinates, the elasticity theory (Mura 1987) tells us that in the cavity

$$\sigma^{el}_{rr}(r) = -\frac{RP}{r^3}\ ,\ \sigma^{el}_{\theta\theta}(r) = \sigma^{el}_{\phi\phi}(r) = \frac{RP}{2r^3} \tag{12}$$

with P the pressure at the cavity surface and R the cavity radius. Figure 2 shows that the computed atomic stress components vary in accordance with elasticity theory, except for short distances due to the presence of the surface. The pressure P in Eq. (12) is the pressure transmitted to the matrix and is an unknown quantity. It is determined by fitting the stress variations with the expression α/r^3, using a range of data for which the influence of the surface on the stress becomes negligible. The analysis of all our data suggests that it is the case when the distance to the surface is greater than 15 Å. Figure 2 shows the result of a fit for tangential components. We checked that fitting the radial stress yields similar result in all cases. The elastic stress tensor $\boldsymbol{\sigma}^{el}$ being known for each atom, the surface stress $\Gamma = (\Gamma_{\theta\theta} + \Gamma_{\phi\phi})/2$ can be computed using Eq. (11).

Surface energy and stress: results

We present in Fig. 3 the results obtained with no applied pressure. The surface energy γ becomes constant when the diameter increases, with the same value for the nanoparticle and the cavity as expected. Although these asymptotic values depend on the selected interatomic potentials, a fair agreement with published values is obtained for Fe (Caro et al. 2011; Stoller and Osetsky 2014; Caro et al. 2015), Al (Jäger et al. 1982), and Si (Eaglesham et al. 1993). Fluctuations can be seen for diameters lower than about 5 nm, although they remain relatively small for Al and Fe. The larger variations for silicon at small diameters is likely due to the random unfinished reconstruction of surfaces with large curvatures. Focusing now on the surface stress Γ, one can see significant variations

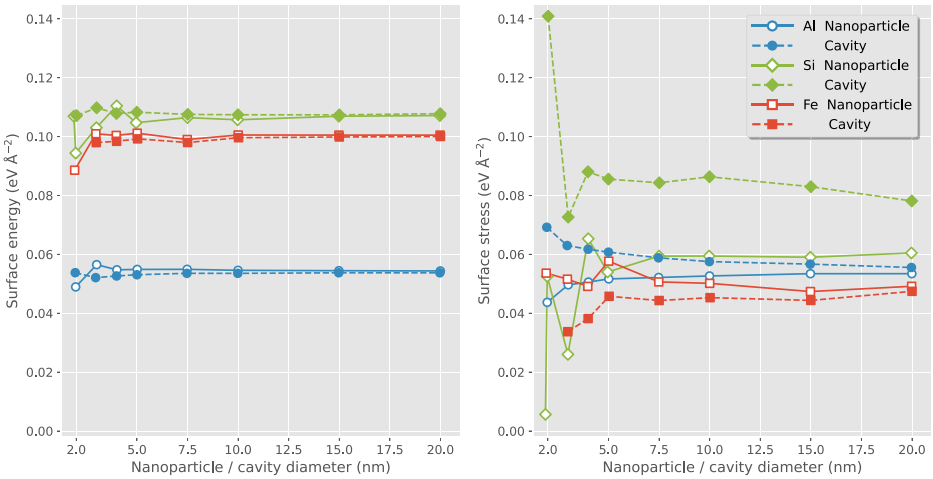

Fig. 3 Surface energy (left) and stress (right) of nanoparticles (open symbols, full lines) and cavities (filled symbols, dashed lines) as a function of their diameter, for aluminum (circles, blue), silicon (diamond, green), and iron (square, red)

depending on the diameter, especially at low diameters (Fig. 3). Values for nanoparticles and cavities at a given diameter can be relatively different, even though the gap tends to slowly wane for the largest systems. For Si and Al, Γ is lower for the nanoparticles than for the cavities, and the opposite is found for Fe. The largest Γ variations are observed for silicon, and the lowest for aluminum. The rationale for these differences between materials is unclear.

It is not surprising to observe these fluctuations for Γ and γ at low diameters, because both quantities depend on the surface structure, which is itself strongly dependent on the size of nanoparticles or cavities. For the largest systems, details of the surface are averaged out and the proportion between the different surface orientations converges to a constant value, i.e., large nanoparticles tend to become all similar. Conversely, structural differences at surfaces are exacerbated for small systems. Then Γ and γ fluctuations are due to the discrete character of surfaces for decreasing diameters, and must not be mistakenly associated with errors coming from the calculation procedure. At last, Tolman proposed that $\gamma \sim \gamma_\infty(1 + \delta/R)$ for decreasing diameters, which is in clear disagreement with our results (Tolman 1949). However we note that this model has been developed for droplets, for which the discrete character of surfaces at small scale does not exist.

Next we discuss the surface energy and stress computed for nanoparticles and cavities in presence of an applied pressure. Before continuing, we describe how the pressure value P can be accurately calculated. P is equal to the sum of the magnitude of the applied forces due to the repulsive force field divided by the nanoparticle/cavity surface. Unfortunately, only the sum of the force vectors is output by LAMMPS. Because of the spherical symmetry, this sum is zero and is then not exploitable for determining the applied pressure. To determine the applied forces due to the force field, we follow this procedure: 1) relax the system for a given applied pressure up to convergence 2) remove the repulsive force field and compute the atomic forces without relaxing the system. These forces are opposed to the forces generated by the repulsive force field according to the third law of Newton. Each computed force vector is next orientated following the technique described in "Nanoparticle" section to obtain its components in spherical coordinates. The applied

pressure can finally be obtained as the sum of the radial force components with $P = \sum F/S$. We checked that the sum of the tangential components is negligible in all cases.

Figure 4 aggregates all results for nanoparticles and cavities of various diameters, for the three materials. Analyzing first nanoparticles and surface energy, we observe an increase with the applied pressure in all cases except for the smallest systems with a 2 nm diameter. For the same reasons as mentioned above, the influence of pressure on surface energy strongly depends on the surface structure at small sizes. This is further demonstrated by considering a second silicon nanoparticle of diameter close to 2 nm, but with a different surface structure (created by slightly shifting the center of the nanoparticle during the generation procedure). The new surface energy is now close to values obtained for larger systems and increases with pressure. A possible cause for the observed surface energy

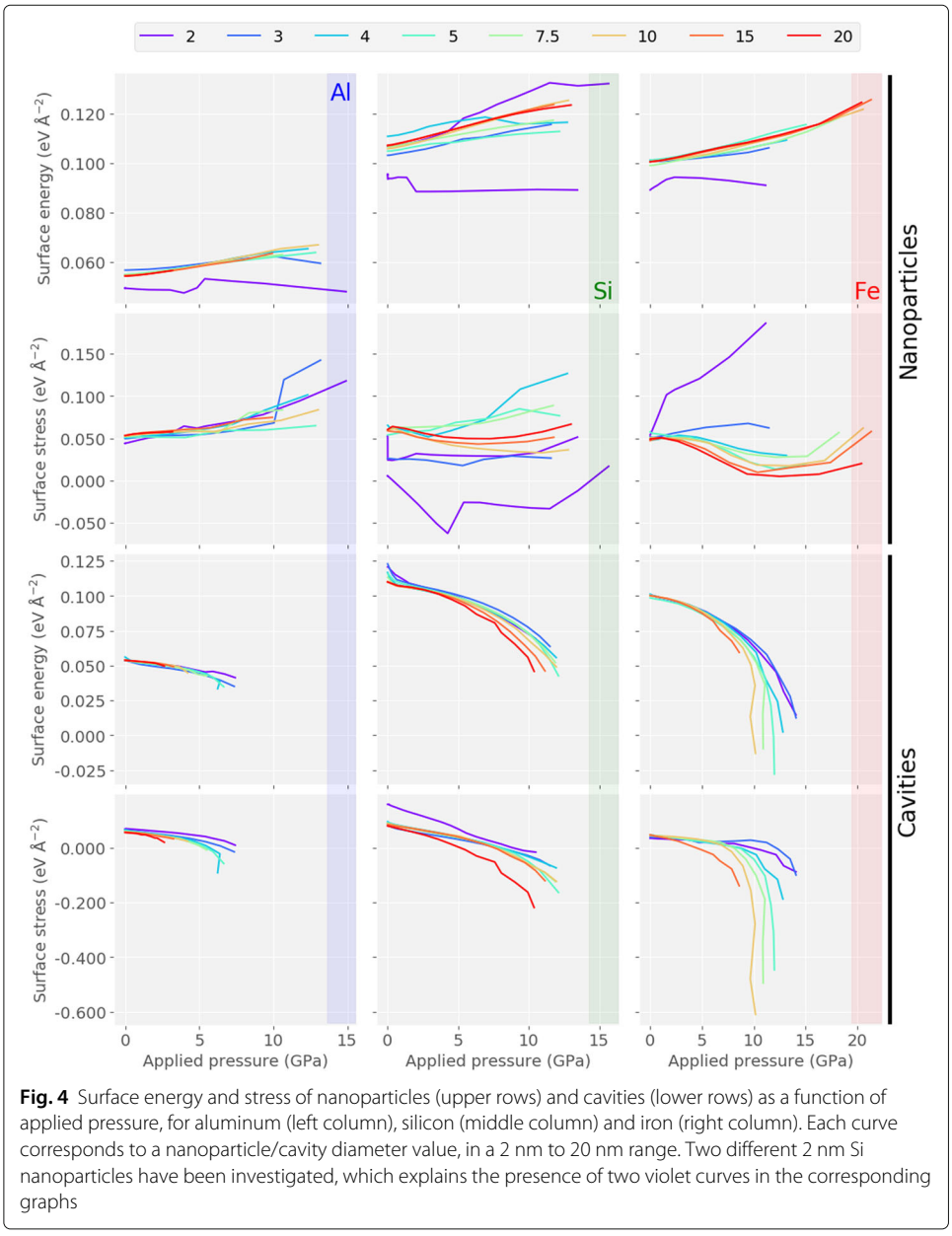

Fig. 4 Surface energy and stress of nanoparticles (upper rows) and cavities (lower rows) as a function of applied pressure, for aluminum (left column), silicon (middle column) and iron (right column). Each curve corresponds to a nanoparticle/cavity diameter value, in a 2 nm to 20 nm range. Two different 2 nm Si nanoparticles have been investigated, which explains the presence of two violet curves in the corresponding graphs

increase is the shrinking of nanoparticles due to compression, which decreases S in Eq. 8. To test this assumption, we have recalculated γ using the S value for the uncompressed relaxed nanoparticles. Results show that the S decrease due to compression is responsible for only 2–5% for Al and Si, and 1–4% for Fe, of the surface energy increase. The origin of the phenomenon is then mainly due to the reduction of the interatomic separations in surface and subsurface layers.

A seemingly more complex picture emerges regarding nanoparticles surface stresses (Fig. 4). Γ increases for Al but remains more or less constant for Si at most diameters (with a significant dispersion). For Fe, Γ first decreases until a plateau is reached, except for the smallest nanoparticles. The contribution due to the decrease of S in Eq. 9 is the same as for the surface energy, i.e., only a few percents. It is difficult to explain these variations using simple physical arguments, as could be done for a slab flat surface.

For cavities, we find that surface energies decrease as a function of the applied pressure in all cases (Fig. 4). In Al, a relatively small drop of 0.02–0.03 eV $Å^{-2}$ at a maximum pressure of 8 GPa is observed, whereas γ in Si is reduced from about 0.11 to 0.04 eV $Å^{-2}$. An even larger drop is found in Fe, with initial values close to 0.1 eV $Å^{-2}$ and decreasing down to -0.028 eV $Å^{-2}$ at 12 GPa. We also find that the lowering rate is proportional to the size of the cavity, in particular for Si and Fe.

The negative γ values for Fe cavities with diameters 7.5–15 nm and high applied pressures might be surprising at first sight, since it suggests that surface creation becomes energetically favored. Actually, analyzing the structure reveals that plastic deformation occurred close to the cavity surface (Fig. 5). In fact, we find that above a pressure threshold, dislocations (in Al and Fe) or amorphous clusters (in Si) nucleate from the surface. These mechanisms are well documented in the literature (Trinkaus 1983; Haghighat et al. 2009; Dérès et al. 2017). The plastic relaxation significantly lowers the applied pressure and the total energy but barely changes the reference energy ε_0 in Eq. (10), thus yielding an apparent negative surface energy. The threshold pressure value depends on the material and on the cavity diameter (Trinkaus 1983; Dérès et al. 2017). Most of the results presented here correspond to pressures below the threshold in order to avoid plasticity, except for the few Fe cases which were kept for illustrating this issue.

The surface stress values as a function of the applied pressure for the cavities are reported in Fig. 4. As for surface energy, Γ is seen to largely decrease when pressure increases, with the greatest reductions for the largest cavities. For instance, Γ is lowered from about 0.08 eV $Å^{-2}$ to -0.22 eV $Å^{-2}$ at 10.3 GPa for a 20 nm cavity in Si. As explained above, the very low surface stress values for Fe cavities with diameters 7.5–15 nm and high applied pressures can be explained by plastic deformation. Finally, we also determined how much the cavity expansion under pressure contributes to surface energy and stress decreases, with the same approach used for nanoparticles. It is found that the variation of S in Eqs. (10)–(11) amounts to about 10%–20% of the lowering. This is significantly higher than for nanoparticles, which can be explained by the dissymmetry between elastic compression and dilatation at high strains. To our knowledge, the influence of pressure on the surface stress in cavities has not been investigated, except in a recent theoretical study of helium bubbles in steel (Jelea 2018). The author reported a surface stress increase as a function of helium pressure, in contrast with our results. The disagreement may originate in the very different conditions for the computations (temperature, presence of helium).

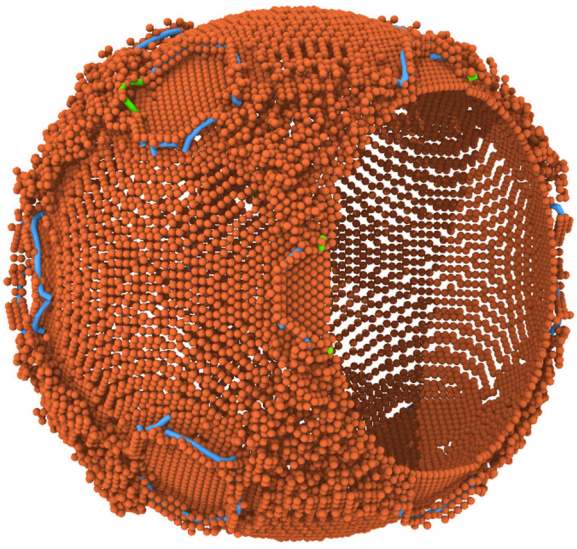

Fig. 5 Relaxed atomic structure of a 15 nm diameter iron cavity with an applied pressure of 10.2 GPa. Only Fe atoms (red spheres) with a coordination number lower than 8 are shown for a better visualization of the cavity external and internal surfaces. A part of the cavity is also cut for sake of clarity. Blue and green tubular lines represent dislocations with ⟨100⟩ and 1/2⟨111⟩ Burgers vectors, respectively, as determined using the dislocation extraction algorithm (Stukowski et al. 2012) implemented in OVITO (Stukowski 2010)

Validity of the Young-Laplace equation

Now that surface energies and stresses are known, the accuracy of the YLE can be studied by comparing ΔP with $2\Gamma/R$ or $2\gamma/R$. First we restrict our investigations to cases with no applied pressures. For a nanoparticle, ΔP in Eq. (1) is equal to P, the pressure in the nanoparticle. P is obtained from atomistic calculations as the trace of the stress tensor in the nanoparticle center. For a cavity, ΔP is equal to $-P$, P being the pressure in the matrix at the cavity surface, determined using Eq. (12). Figure 6, top left graph, shows the absolute value of the difference (sum) between P and the Laplace pressure as a function of nanoparticle (cavity) diameter. The closer the values to zero the more accurate the YLE. If the Laplace pressure is computed using $\gamma(D)$, the diameter dependent surface energy, the curves in the top left graph of Fig. 6 are obtained. For the smallest Si and Fe nanoparticles, the values can be greater than 1–2 GPa. They become lower than 0.5 GPa for diameters greater than 7.5 nm. We emphasize that seeing the slow decline for Si and Fe as a convergence is misleading, since both ΔP and the Laplace pressure also decrease for growing diameters. As a workaround one can consider the relative error $(|\Delta P - 2\gamma/R)/\Delta P|$. For Si and Fe, this quantity remains close to 100% for all diameters. However it is smaller for Al, being about 10% for the smallest nanoparticles and decreasing down to 0.01% for the largest one. Now if the surface stress is used to compute the Laplace pressure, the values are overall lowered compared to the surface energy (Fig. 6, top right graph). In fact, it is significantly smaller for Fe and Si, and marginally greater for Al. For large diameters, the values are close to zero for all materials. In addition, we find that the relative error is now close or lower than 10% in most cases, which further confirms the conclusion in Ref. Jelea (2018) that surface stress should be used to compute the Laplace pressure in the YLE, and not surface energy.

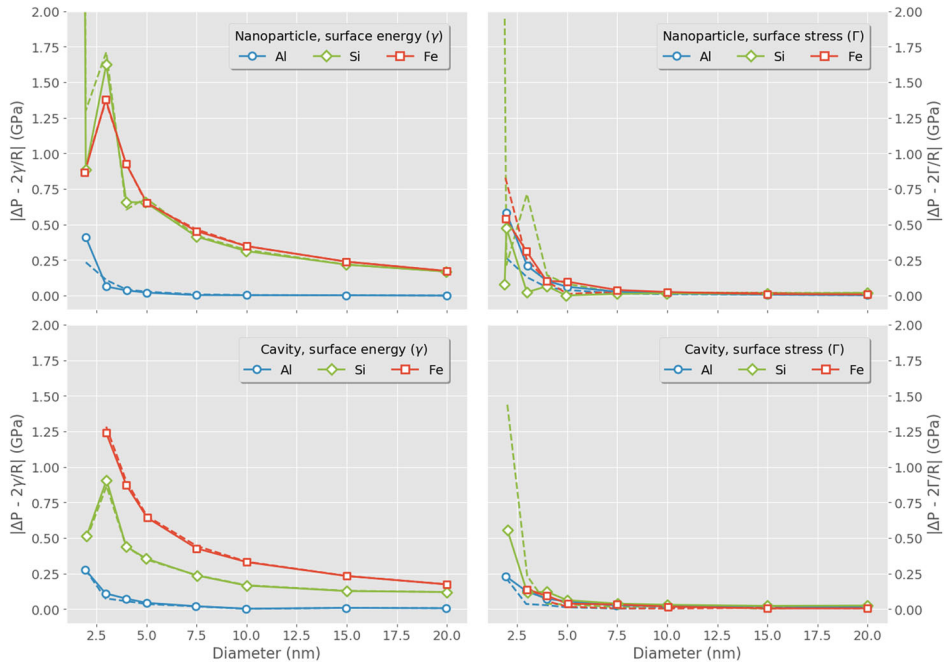

Fig. 6 Absolute difference between the pressure calculated in the nanoparticle or in the vicinity of the cavity, and the Laplace pressure as a function of the nanoparticle/cavity diameter, with no extra applied pressure. Top (bottom) graphs show results for nanoparticles (cavities). The Laplace pressure is computed using either surface energy γ (left graphs) or surface stress Γ (right graphs). Full lines with symbols show results obtained with γ or Γ values corresponding to each diameter, while values at diameters equal to 20 nm are used to obtain data associated with dashed lines

For cavities, the results are similar (Fig. 6, bottom graphs). With surface energy, the values are the highest for small Fe cavities, about 1.25 GPa, and a slow decrease as a function of diameter is observed for Fe and Si. Again, the lowest values correspond to aluminum. Relative errors are roughly 1–10% (Al), 30–50% (Si), and 100% (Fe). Using surface stress, both absolute and relative errors are substantially lowered, except for Al. For instance the relative error ranges between 2% and 10% for all materials and all sizes. Finally, we also evaluate the influence of using a constant value instead of diameter dependent data. The dashed lines in Fig. 6 show the variation of the same quantities than for full lines, but calculated with a constant value of the surface energy/stress taken for a 20 nm diameter nanoparticle/cavity. We find significant differences only for small systems and when surface stress is used. This is in agreement with the previously made conclusion that surface energy is weakly dependent on diameter, unlike surface stress.

Second, the accuracy of the YLE with respect to the nanoparticle/cavity diameter in presence of an applied pressure is investigated. ΔP in Eq. (1) is now equal to $P - P_{\text{appl}}$ for the nanoparticle (or to $P_{\text{appl}} - P$ for the cavity), with P_{appl} the applied pressure. To determine the Laplace pressure, we consider different possible options: use (i) a constant surface energy (the one calculated for the largest system, $D = 20$ nm, with no applied pressure), (ii) the diameter dependent surface energy with no applied pressure, (iii) the diameter dependent pressure dependent surface energy, (iv) the constant surface stress calculated for the largest system ($D = 20$ nm) with no applied pressure, (v) the diameter dependent surface stress with no applied pressure, (vi) the diameter dependent pressure

dependent surface stress. Each of these choices is a priori better that the one customarily made in the literature, that is using a value close or averaged from flat surface energies. Figure 7-a represents the difference between ΔP and the Laplace pressure for all investigated nanoparticles, for option (i). Most of the values appear close to zero suggesting a good accuracy for the YLE. However, the scale of the figure is deceptive, and errors of several tenths of GPa are obtained in numerous cases. Furthermore, much larger deviations are visible, especially for the smallest nanoparticles at high applied pressures. These results can be compared to those obtained using pressure and diameter dependent surface stress, option (vi), shown in Fig. 7-b. A dramatic reduction in scatter is observed for all diameters and applied pressures, even if a significant dispersion remains for a few data points corresponding to the smallest nanoparticles, with errors of about 1–2 GPa. To be more quantitative, we plot in Fig. 7-c the standard deviation corresponding to data distributions computed following options (i)-(vi), as a rough indicator of the accuracy of the

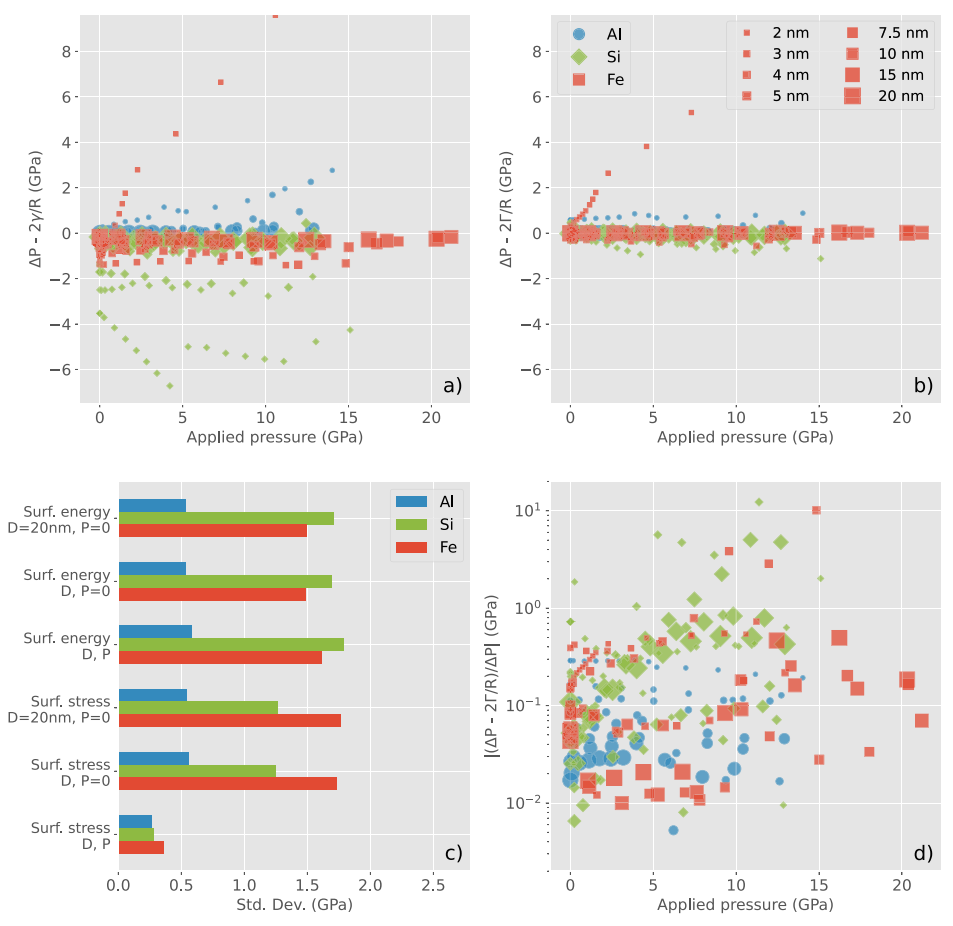

Fig. 7 a) Difference between ΔP and the Laplace pressure for nanoparticles as a function of the applied pressure (Blue circles: Al, green diamond: Si, red squares: Fe). The symbol size is proportional to the diameter. The surface energy of the 20 nm diameter nanoparticle is used to calculate the Laplace pressure. b) same quantity and representation than in a), except that the diameter and pressure dependent surface stress value is now used to compute the Laplace pressure. c) Standard deviation for differences between ΔP and the Laplace pressure for nanoparticles. Each set of bars corresponds to a specific choice for the surface energy/stress used to compute the Laplace pressure (see text for details). d): Relative difference between ΔP and the Laplace pressure for nanoparticles as a function of the applied pressure, using the diameter and pressure dependent surface stress value

YLE. One can see that there are little differences between the first five sets, with almost constant values for Al and Fe. A spectacular reduction of the standard deviation is however achieved when the size and pressure dependent surface stress is used, confirming the visual impression between Fig. 7-a and -b. For these specific conditions, the relative error is represented in Fig. 7-d. For aluminum, we find an error range between 1% and 10% for most data, with maxima as high as 30% for the smallest nanoparticles. Larger errors are obtained for iron, from 1% to about 100%. Finally, the poorest accuracy corresponds to silicon, with errors between 10% and 100% for a majority of data, and as high as 1000% for several cases. Therefore even if a significant improvement is obtained using the diameter and pressure dependent surface stress in the YLE, the predicted pressures can largely deviate from the true values, especially in presence of an applied pressure.

A similar analysis is made for cavities. As for nanoparticles, we first examine the results obtained when using the surface energy calculated for a 20 nm cavity and no applied pressure (Fig. 8-a). We find an increasing deviation towards negative values as pressure grows, for all three materials, and the effect seems overall stronger for small cavities. The reason for this is not clear. A significant improvement is achieved by using diameter and pressure dependent surface stress to compute the Laplace pressure (Fig. 8-b). Although data are now closer to zero, the distribution tail at high applied pressures slightly deflects upwards. The standard deviations for the different options (i)-(vi), shown in Fig. 8-c, reveal a similar scenario than for nanoparticles. In fact the best result is undoubtedly achieved when diameter and pressure dependent surface stress is used to compute the Laplace pressure. Finally, we analyze the relative error in these conditions (Fig. 8-d). For an applied pressure lower than 5 GPa, the estimated error can be lower than 1% and as high as 100%. Very low errors are obtained for small Si or Al cavities, whereas most data for iron correspond to errors greater than 10%. The errors grow as a function of the applied pressure for all materials, ranging approximately from 10% to 1000% for pressures higher than 8 GPa.

Concluding remarks

In this work, we developed methods allowing for the calculation of the surface energy and stress of nanoparticles and cavities from interatomic potential calculations. They make use of elasticity theory in the case of cavities, but not for nanoparticles. These methods are next applied to investigate the variation of surface energy/stress as a function of the size of a nanoparticle/cavity, in presence or not of an applied pressure, for aluminum, silicon, and iron. The results are used to study the accuracy of the YLE, as a function of these parameters.

Our investigations produced original results and brought forward several conclusions. Concerning surface energy and stress, we determined the critical sizes below which the discrete character of surfaces can not be ignored. These are close to 4–5 nm for surface energy, and greater for surface stress. The larger surface influence is obtained for silicon as expected. We find that surface energy and stress slightly increase as a function of pressure in the case of nanoparticles. A much stronger and opposite effect is obtained for cavities, the decrease leading to negative values at high pressure. We correlate this sign reversal with the failure of surface caused by plastic deformation. Dislocation loop punching is then demonstrated for pressurized cavities in iron (Haghighat et al. 2009).

An analysis of the accuracy of the YLE is made by computing independently each term in Eq. (1). With no applied pressure, we find that the error is at most 20% for nanoparticle

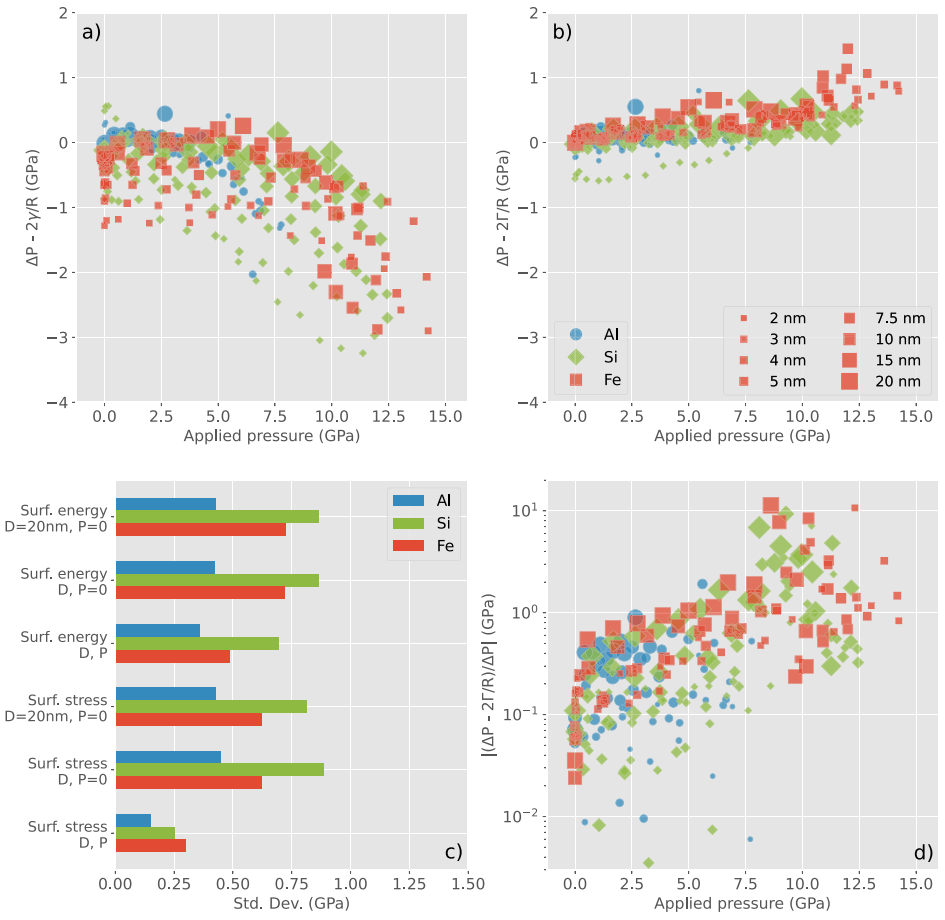

Fig. 8 a) Difference between ΔP and the Laplace pressure for cavities as a function of the applied pressure (Blue circles: Al, green diamond: Si, red squares: Fe). The symbol size is proportional to the diameter. The surface energy of the 20 nm diameter cavity is used to calculate the Laplace pressure. b) same quantity and representation than in a), except that the diameter and pressure dependent surface stress value is now used to compute the Laplace pressure. c) Standard deviation for differences between ΔP and the Laplace pressure for cavities. Each set of bars corresponds to a specific choice for the surface energy/stress used to compute the Laplace pressure (see text for details). d): Relative difference between ΔP and the Laplace pressure for cavities as a function of the applied pressure, using the diameter and pressure dependent surface stress value

sizes greater than 4 nm (2 nm for cavities). However, this accuracy is only obtained when diameter dependent surface stresses are used to calculate the Laplace pressure. If surface energy, even with size dependent values, is used instead, the accuracy considerably worsens, with errors up to 100%. We reach a similar conclusion when an applied pressure is present. In fact, the lowest errors are obtained when diameter and pressure dependent surface stress values are used. The error is typically lower than 50% for pressures up to 5 GPa in nanoparticles, with the best accuracy for aluminum. For cavities, the errors range from about 10% to 100% for pressures below 5 GPa, but can be as high as 1000% for larger pressures.

Our investigations then show that the YLE should not be used to obtain accurate pressure values for nanoparticles or cavities, especially when the Laplace pressure is computed with a constant surface energy as it is customarily done in the literature. The precision can be systematically improved by using surface stress instead. However, its value is also

shown to depend on the size and the pressure, in agreement with a recent work (Jelea 2018). This raises questions about the extent to which one can use the YLE to analyze the state of highly pressurized bubbles in a nuclear context. Another important point concerns the minimum size below which the validity of YLE is clearly questionable. This size is estimated to be a few nanometers for nanoparticles, and slightly smaller for cavities. This is in agreement with previous works (Hawa and Zachariah 2004; Cui et al. 2015). Below this threshold the discrete character of surfaces cannot be neglected. The assumption of sphericity used in this work is also less appropriate at small sizes. And it becomes increasingly difficult to extract accurate surface stress data in the smallest nanoparticles, for which all atoms are close to the surface. For cavities, the use of a continuum theory like elasticity theory to determine the surface stress also becomes questionable at such sizes. Furthermore, in this work we used isotropic elasticity theory, which is maybe not best suited for anisotropic materials like iron or silicon. From this perspective, it would be interesting to see whether improved results could be obtained by using anisotropic elasticity theory.

Acknowledgements
The authors would like to thank Prof. Pierre Müller for his critical reading of the manuscript and his insightful comments.

Authors' contributions
L.P. performed the atomistic simulations. L.P. and M.-L.D discussed the results together and contributed to the writing of the paper. The authors read and approved the final manuscript.

Funding
This work was supported by the French government program "Investissements d'Avenir" (EUR INTREE, reference ANR-18-EURE-0010). Computations have been performed using the supercomputer facilities of the Mésocentre de calcul Poitou-Charentes.

Availability of data and materials
The data that support the findings of this study are available from the corresponding author upon reasonable request.

Declarations

Competing interests
The authors declare that they have no competing interests.

Received: 31 March 2021 Accepted: 21 July 2021
Published online: 03 September 2021

References

K. Alix, M.-L. David, J. Dérès, C. Hébert, L. Pizzagalli, Evolution of the properties of helium nanobubbles during in situ annealing probed by spectrum imaging in the transmission electron microscope. Phys. Rev. B. **97**(10), 104102 (2018). https://doi.org/10.1103/physrevb.97.104102

K. Alix, M.-L. David, G. Lucas, D. T. L. Alexander, F. Pailloux, C. Hébert, L. Pizzagalli, Gentle quantitative measurement of helium density in nanobubbles in silicon by spectrum imaging. Micron. **77**, 57–65 (2015). https://doi.org/10.1016/j.micron.2015.05.011

P. Armstrong, W. Peukert, Size effects in the elastic deformation behavior of metallic nanoparticles. J. Nanoparticle Res. **14**(12), 1288 (2012). https://doi.org/10.1007/s11051-012-1288-4

A. Aslanides, V. Pontikis, Atomistic study of dislocation cores in aluminium and copper. Comput. Mater. Sci. **10**(1), 401–405 (1998)

F. Bai, K. Bian, X. Huang, Z. Wang, H. Fan, Pressure induced nanoparticle phase behavior, property, and applications. Chem. Rev. **119**(12), 7673–7717 (2019)

S. Bel Haj Salah, C. Gerard, L. Pizzagalli, Influence of surface atomic structure on the mechanical response of aluminum nanospheres under compression. Comput. Mater. Sci. **129**, 273–278 (2017). https://doi.org/10.1016/j.commatsci.2016.12.033

E. Bitzek, P. Koskinen, F. Gähler, M. Moseler, P. Gumbsch, Structural relaxation made simple. Phys. Rev. Lett. **97**, 170201 (2006)

R. C. Cammarata, Surface and interface stress effects in thin films. Prog. Surf. Sci. **46**(1), 1–38 (1994). https://doi.org/10.1016/0079-6816(94)90005-1

A. Caro, J. Hetherly, A. Stukowski, M. Caro, E. Martinez, S. Srivilliputhur, L. Zepeda-Ruiz, M. Nastasi, Properties of helium bubbles in Fe and FeCr alloys. J. Nucl. Mater. **418**(1-3), 261–268 (2011). https://doi.org/10.1016/j.jnucmat.2011.07.010

A. Caro, D. Schwen, J. Hetherly, E. Martinez, The capillarity equation at the nanoscale: Gas bubbles in metals. Acta Mater. **89**, 14–21 (2015). https://doi.org/10.1016/j.actamat.2015.01.048

J. Cui, M. Li, J. Wang, Q. Hou, Molecular dynamics study of helium bubble pressure in tungsten. Nucl. Inst. Methods Phys. Sect. Res. B: Beam Interact. Mater. Atoms. **352**, 104–106 (2015). Proceedings of the 12th International Conference on Computer Simulation of Radiation Effects in Solids, Alacant, Spain, 8-13 June, 2014

M.-L. David, K. Alix, F. Pailloux, V. Mauchamp, M. Couillard, G. A. Botton, L. Pizzagalli, In situ controlled modification of the helium density in single helium-filled nanobubbles. J. Appl. Phys.s. **115**(12), 123508 (2014). https://doi.org/10.1063/1.4869213

J. Dérès, M.-L. David, K. Alix, C. Hébert, D. T. L. Alexander, L. Pizzagalli, Properties of helium bubbles in covalent systems at the nanoscale: A combined numerical and experimental study. Phys. Rev. B. **96**, 014110 (2017). https://doi.org/10.1103/PhysRevB.96.014110

D. J. Eaglesham, A. E. White, L. C. Feldman, N. Moriya, D. C. Jacobson, Equilibrium shape of Si. Phys. Rev. Lett. **70**(11), 1643 (1993)

S. Fréchard, M. Walls, M. Kociak, J. P. Chevalier, J. Henry, D. Gorse, Study by eels of helium bubbles in a martensitic steel. J. Nucl. Mater. **393**, 102 (2009)

S. M. H. Haghighat, G. Lucas, R. Schäublin, State of a pressurized helium bubble in iron. Europhys. Lett. **85**, 60008 (2009)

T. Hawa, M. R. Zachariah, Internal pressure and surface tension of bare and hydrogen coated silicon nanoparticles. J. Chem. Phys. **121**(18), 9043–9049 (2004). https://doi.org/10.1063/1.1797073

P. Hecquet, Surface stresses on symmetric (2×1) reconstructed si(001) calculated from surface energy variations. Surf. Sci. **618**, 83–87 (2013). https://doi.org/10.1016/j.susc.2013.08.008

J. P. Hirth, J. Lothe, *Theory of Dislocations*. (Wiley, New York, 1982)

W. Jäger, R. Manzke, H. Trinkaus, G. Crecelius, R. Zeller, J. Fink, H. L. Bay, Density and pressure of helium in small bubbles in metals. J. Nucl. Mater. **111-112**, 674–680 (1982). https://doi.org/10.1016/0022-3115(82)90288-4

A. Jelea, On the laplace-young equation applied to spherical fluid inclusions in solid matrices. J. Nucl. Mater. **505**, 127–133 (2018). https://doi.org/10.1016/j.jnucmat.2018.03.051

Q. Jiang, L. H. Liang, D. S. Zhao, Lattice contraction and surface stress of fcc nanocrystals. J. Phys. Chem. B. **105**(27), 6275–6277 (2001). https://doi.org/10.1021/jp010995n

R. Lazzari, J. Goniakowski, G. Cabailh, R. Cavallotti, N. Trcera, P. Lagarde, J. Jupille, Surface and epitaxial stresses on supported metal clusters. Nanoletters. **16**(4), 2574–2579 (2016). https://doi.org/10.1021/acs.nanolett.6b00143

B. Luan, M. O. Robbins, The breakdown of continuum models for mechanical contacts. Nature. **435**, 929 (2005)

W. Luo, W. Hu, Gibbs free energy, surface stress and melting point of nanoparticle. Phys. B. **425**, 90–94 (2013). https://doi.org/10.1016/j.physb.2013.05.025

P. Maioli, T. Stoll, H. E. Sauceda, I. Valencia, A. Demessence, F. Bertorelle, A. Crut, F. Vallée, I. L. Garzón, G. Cerullo, N. D. Fatti, Mechanical vibrations of atomically defined metal clusters: From nano- to molecular-size oscillators. Nanoletters. **18**(11), 6842–6849 (2018). https://doi.org/10.1021/acs.nanolett.8b02717

L. Makkonen, Misinterpretation of the shuttleworth equation. Scr. Mater. **66**(9), 627–629 (2012). https://doi.org/10.1016/j.scriptamat.2012.01.055

B. Medasani, Y. H. Park, I. Vasiliev, Theoretical study of the surface energy, stress, and lattice contraction of silver nanoparticles. Phys. Rev. B. **75**(23), 235436 (2007). https://doi.org/10.1103/physrevb.75.235436

P. Müller, A. Saùl, Elastic effects on surface physics. Surf. Sci. Rep. **54**(5-8), 157–258 (2004). https://doi.org/10.1016/j.surfrep.2004.05.001

P. Müller, A. Saùl, F. Leroy, Simple views on surface stress and surface energy concepts. Adv. Nat. Sci.: Nanosci. Nanotech. **5**(1), 013002 (2014). https://doi.org/10.1088/2043-6262/5/1/013002

T. Mura, *Micromechanics of Defects in Solids*, 2nd edn. (Martinus Nijhoff Publishers, Dordrecht, The Netherlands, 1987)

R. J. Needs, Calculations of the surface stress tensor at aluminum (111) and (110) surfaces. Phys. Rev. Lett. **58**(1), 53–56 (1987). https://doi.org/10.1103/physrevlett.58.53

K. Ono, M. Miyamoto, H. Kurata, M. Haruta, A. Yatomi, Dynamic behavior of helium bubbles at high temperature in Si studied by in situ TEM, STEM-EELS, and TDS. J. Appl. Phys. **126**(13), 135104 (2019). https://doi.org/10.1063/1.5118684

M. C. Payne, N. Roberts, R. J. Needs, M. Needels, J. D. Joannopoulos, Total energy and stress of metal and semiconductor surfaces. Surf. Sci. **211/212**, 1 (1989)

L. Pizzagalli, A. Charaf-Eddin, S. Brochard, Numerical simulations and modeling of the stability of noble gas atoms in interaction with vacancies in silicon. Comput. Mater. Sci. **95**, 149–158 (2014). https://doi.org/10.1016/j.commatsci.2014.07.011

L. Pizzagalli, J. Godet, J. Guénolé, S. Brochard, E. Holmstrom, K. Nordlund, T. Albaret, A new parametrization of the stillinger-weber potential for an improved description of defects and plasticity of silicon. J. Phys. Condens. Matter. **25**(5), 055801 (2013)

S. Plimpton, Fast parallel algorithms for short-range molecular dynamics. J. Comput. Phys. **117**(1), 1–19 (1995)

L. Proville, D. Rodney, M.-C. Marinica, Quantum effect on thermally activated glide of dislocations. Nat. Mater. **11**, 845 (2012)

R. Schierholz, B. Lacroix, V. Godinho, J. Caballero-Hernández, M. Duchamp, A. Fernández, Stem–eels analysis reveals stable high-density he in nanopores of amorphous silicon coatings deposited by magnetron sputtering. Nanotechnology. **26**(7), 075703 (2015)

R. Shuttleworth, The surface tension of solids. Proc. Phys. Soc. Sect. A. **63**(5), 444–457 (1950). https://doi.org/10.1088/0370-1298/63/5/302

R. E. Stoller, Y. N. Osetsky, An atomistic assessment of helium behavior in iron. J. Nucl. Mater. **455**(1–3), 258–262 (2014). https://doi.org/10.1016/j.jnucmat.2014.06.020. Proceedings of the 16th International Conference on Fusion Reactor Materials (ICFRM-16)

A. Stukowski, Visualization and analysis of atomistic simulation data with OVITO-the Open Visualization Tool. Model. Simul. Mater. Sci. Eng. **18**(1), 015012 (2010). https://doi.org/10.1088/0965-0393/18/1/015012

A. Stukowski, V. V. Bulatov, A. Arsenlis, Automated identification and indexing of dislocations in crystal interfaces. Model. Simul. Mater. Sci. Eng. **20**(8), 085007 (2012). https://doi.org/10.1088/0965-0393/20/8/085007

S. Swaminarayan, R. Najafabadi, D. J. Srolovitz, Polycrystalline surface properties from spherical crystallites: Ag, Au, Cu and Pt. Surf. Sci. **306**(3), 367–380 (1994). https://doi.org/10.1016/0039-6028(94)90078-7

A. Tanguy, F. Leonforte, J. P. Wittmer, J. L. Barrat, Vibrations of amorphous nanometric structures: when does the classical continuum theory apply? Appl. Surf. Sci. **226**, 282–288 (2004)
D. Taverna, M. Kociak, O. Stéphan, A. Fabre, E. Finot, B. Décamps, C. Colliex, Probing physical properties of confined fluids within individual nanobubbles. Phys. Rev. Lett. **100**, 035301 (2008)
A. P. Thompson, S. J. Plimpton, W. Mattson, General formulation of pressure and stress tensor for arbitrary many-body interaction potentials under periodic boundary conditions. J. Chem. Phys. **131**(15), 154107 (2009). https://doi.org/10.1063/1.3245303
S. Timoshenko, J. N. Goodier, *Theory of Elasticity*. (McGraw-Hill, New-York, 1951)
R. C. Tolman, The effect of droplet size on surface tension. J. Chem. Phys. **17**(3), 333–337 (1949). https://doi.org/10.1063/1.1747247
H. Trinkaus, Energetics and formation kinetics of helium bubbles in metals. Radiat. Eff. **78**, 189 (1983)
M. Vergeles, A. Maritan, J. Koplik, J. R. Banavar, Adhesion of solids. Phys. Rev. E. **56**(3), 2626–2634 (1997). https://doi.org/10.1103/PhysRevE.56.2626
W. G. Wolfer, Elastic properties of surfaces on nanoparticles. Acta Mater. **59**(20), 7736–7743 (2011). https://doi.org/10.1016/j.actamat.2011.08.033
L. Yang, J.-J. Bian, G.-F. Wang, Impact of atomic-scale surface morphology on the size-dependent yield stress of gold nanoparticles. J. Phys. D: Appl. Phys. **50**, 245302 (2017)

Publisher's Note